American Journal of Epidemiology

Vol. 189, No. 9
DOI: 10.1093/aje/kwaa023
Advance Access publication:
February 20, 2020

Study Design

Microvascular Phenotyping in the Maastricht Study: Design and Main Findings, 2010–2018

Wenjie Li, Miranda T. Schram, Ben M. Sörensen, Marnix J. M. van Agtmaal, Tos T. J. M. Berendschot, Carroll A. B. Webers, Jacobus F. A. Jansen, Walter H. Backes, Ed H. B. M. Gronenschild, Casper G. Schalkwijk, Coen D. A. Stehouwer, and Alfons J. H. M. Houben*

*Correspondence to Dr. Alfons J. H. M. Houben, Department of Internal Medicine and School for Cardiovascular Diseases, Maastricht University Medical Center+, P. Debyelaan 25, Maastricht, 6229 HX, the Netherlands (e-mail: b.houben@maastrichtuniversity.nl).

Initially submitted May 17, 2019; accepted for publication February 17, 2020.

Microvascular dysfunction (MVD) is a common pathophysiological change that occurs in various diseases, such as type 2 diabetes mellitus (T2DM), heart failure, dementia, and depression. Recent technical advances have enabled noninvasive measurement and quantification of microvascular changes in humans. In this paper, we describe the protocols of the microvascular measurements applied in the Maastricht Study, an ongoing prospective, population-based cohort study of persons aged 40–75 years being carried out in the southern part of the Netherlands (baseline data assessment, November 2010–January 2020). The study includes a variety of noninvasive measurements in skin, retina, brain, and sublingual tissue, as well as plasma and urine biomarker assessments. Following this, we summarize our main findings involving these microvascular measurements through the end of 2018. Finally, we provide a brief perspective on future microvascular investigations within the framework of the Maastricht Study.

cardiovascular disease; microvascular dysfunction; pathophysiology; population-based studies; type 2 diabetes

Abbreviations: MRI, magnetic resonance imaging; MVD, microvascular dysfunction; RBC, red blood cell; SMF, skin microvascular flowmotion; T2DM, type 2 diabetes mellitus; WMH, white matter hyperintensity.

Microvascular dysfunction (MVD) is involved in the development and progression of various diseases, such as type 2 diabetes mellitus (T2DM), heart failure, dementia, and depression (1–8). The microcirculation performs essential functions in both physiological and pathophysiological states, including delivery of oxygen and nutrients, removal of waste, heat exchange with the environment, assistance in endocrine system communication, blood pressure regulation, and immune response (9–12). Investigation of microvascular function can thus expand our knowledge of the pathophysiology of different diseases.

Nowadays, state-of-the-art technologies enable assessment of both structural and functional aspects of the human microcirculation in different regions (13–21). Introducing these measurements in a population-based setting permits the study of microvascular changes that occur in various diseases, as well as their similarities and differences across various territories. Additionally, the description of measurement protocols is necessary in order to identify whether differences in results across studies are based on differences in methodology.

The general design of the Maastricht Study, a population-based cohort study, has been described previously (22). In the present paper, we describe a wide range of microvascular measurements that have been implemented gradually in the Maastricht Study and provide a summary of the main findings and perspectives on microvascular phenotyping, with an update through the end of 2018.

METHODS

A detailed description of the study population and design of the Maastricht Study can be found in the Web Appendix (available at https://academic.oup.com/aje) and a previous

paper (22). The Maastricht Study is an ongoing observational, prospective, population-based cohort study. All residents of the southern part of the Netherlands aged 40–75 years are eligible for participation. Baseline data assessment took place from November 2010 to January 2020. Table 1 gives an overview of all microvascular measurements and corresponding variables used to assess microvascular (dys)function that have been implemented in the Maastricht Study. Microvascular measurements applied from the onset of the study include skin capillary density and recruitment, skin flowmotion, and biomarkers of endothelial function obtained from plasma and urine samples. Measurements of heat-induced skin hyperemic response, retinal static and dynamic measurements, and magnetic resonance imaging (MRI) measurements were introduced after approximately 8, 11, and 13 months, respectively. Lastly, measurement of endothelial glycocalyx thickness was introduced 22 months after initiation of the study. Data collection in the Maastricht Study and validation of the microvascular measurements are described in the Web Appendix.

Retinal microvascular reactivity

The retinal microvascular dilation response to flicker light, which is related to nutritive demands of activated retinal neurons and is nitric-oxide–dependent (16, 23), is measured in a dimly lit room using the Dynamic Vessel Analyzer (Imedos Systems GmbH, Jena, Germany). Mydriasis is induced with 2 drops of tropicamide (0.5%) and 1 drop of phenylephrine (2.5%) 15 minutes prior to the Dynamic Vessel Analyzer measurements. For safety reasons, participants with an intraocular pressure exceeding 30 mm Hg are excluded from retinal measurements. Per participant, we randomly measure the left or right eye.

During the measurement, the participant is instructed to focus on the tip of a fixed needle inside the retinal camera (FF450; Carl Zeiss AG, Jena, Germany) while the fundus of the eye is examined under green measuring light (530–600 nm; illumination of fundus approximately 6,500 lux). Straight arteriolar and venular segments of approximately 1.5 mm in length located 0.5–2.0 disc diameters from the margin of the optic disc in the temporal section are examined (Figure 1A, left panel, zone "b").

After the specific vessel profile is recognized, its diameter is automatically and continuously measured for 150 seconds. A baseline recording of 50 seconds is followed by a 40-second flicker light exposure period (flicker frequency 12.5 Hz (24), bright:dark contrast ratio 25:1) and a subsequent 60-second recovery period (Figure 1A, right panel). We use a 40-second flicker light stimulation based on the findings of Nagel et al. (25) and Kotliar et al. (26), who observed that healthy individuals exhibited maximum dilation immediately after the 20-second flicker stimulation, whereas the time to maximal arteriolar dilation of obese individuals was prolonged. We have chosen to perform a single cycle of 40-second flicker light stimulation because of time restraints for the large amount of measurements in the Maastricht Study. Notably, despite a difference in flicker duration, the average arteriolar/venular percent-dilation responses we observe are comparable to those in studies using 3 cycles of short flicker light stimulation. The Dynamic Vessel Analyzer automatically corrects for alterations in luminance caused by, for example, slight eye movements. During blinks and small eye movements, the registration stops, and it restarts once the vessel segments are automatically reidentified (16).

The integrated Dynamic Vessel Analyzer software (version 4.51; Imedos Systems) automatically calculates baseline diameter and percentage dilation. Baseline diameter is calculated as the average diameter size of the 20- to 50-second recording and is expressed in measurement units, where 1 measurement unit is equal to 1 μm of the Gullstrand eye (27). Percentage dilation over baseline is based on the average dilation achieved at the time points 10 seconds and 40 seconds during the flicker stimulation period. Two regression lines are drawn (at intervals of 0–<10 seconds and 10–40 seconds during flicker stimulation), and results are averaged to assess average percentage of dilation. The purpose of taking the average dilation is to account for interindividual variation in the curve shape during dilation.

Retinal microvascular diameters and morphology

State-of-the-art technology enables quantification and analysis of various features of retinal microvasculature (semi)automatically (e.g., vascular diameters, tortuosity, fractal dimension, and bifurcation features (Figure 1A, left panel). In the Maastricht Study, fundus photography of both eyes is performed 15 minutes after the pupils have been dilated with tropicamide 0.5% and phenylephrine 2.5%. All fundus photographs are made with a focus, shot, and tracker fundus camera (model AFC-230; Nidek Co. Ltd., Aichi, Japan) in 45 degrees of at least 3 fields: 1 field centered on the optic disc, 1 field centered on the macula, and 1 temporal field positioned 1 disc diameter from the center of the macula.

Static retinal vessel analysis is performed with the RHINO software developed by the RetinaCheck Project group at the Eindhoven University of Technology (Eindhoven, the Netherlands) (17,18). Retinal vessel diameters are measured 0.5–1.0 disc diameter away from the optic disc margin and 1.0–1.5 disc diameter away from the fovea (macula) center (zone "a"), while retinal vascular tortuosity, retinal fractal dimension, and bifurcation-based features are studied within 1.0–2.5 disc diameters (zone "b") and 1.0–3.0 disc diameters (zone "c") from the optic disc center or fovea (macula) center, respectively (Figure 1A, left panel). The scale factor is based on the optic disc diameter, which is assumed to be 1,800 μm (28).

Retinal vessel diameters are presented as central retinal arteriolar equivalent and central retinal venular equivalent. Central retinal arteriolar equivalent and central retinal venular equivalent represent the equivalent single-vessel parent diameters for the 6 largest arterioles and largest venules in the region of interest, respectively. The calculations are based on the improved Knudtson-Hubbard formula (29).

Retinal microvascular morphology includes retinal microvascular tortuosity, fractal dimension, and bifurcation-

Table 1. Microvascular Measurements Taken in the Maastricht Study, Maastricht, the Netherlands, 2010–2018

Measurement	Technique	Variable(s)	Units
Skin capillary density and recruitment	Videomicroscopy	Baseline capillary density	No./mm^2
		Capillary recruitment following arterial occlusion	No./mm^2, %
		Capillary density during venous congestion	No./mm^2, %
Skin flowmotion	Laser Doppler flowmetry	Total skin microvascular flowmotion power density	AU
		Skin flowmotion component power density[a]	AU
		Endothelial component (0.01–0.02 Hz)	
		Neurogenic component (0.02–0.06 Hz)	
		Myogenic component (0.06–0.15 Hz)	
		Respiratory component (0.15–0.40 Hz)	
		Cardiac component (0.40–1.60 Hz)	
Skin heating response	Laser Doppler flowmetry	Skin baseline blood flow	PU
		Heat-induced skin average hyperemia	PU, %
Retinal microvascular reactivity	Videomicroscopy	Retinal arteriolar/venular baseline diameter	MU
		Flicker light-induced retinal arteriolar/venular average dilation	MU, %
Retinal microvascular diameters and morphology	Fundus photography	Calibers	
		Central retinal arteriolar/venular equivalent	MU
		Arteriole:venule ratio	Unitless
		Tortuosity	
		Arteriolar/venular tortuosity	Unitless
		Fractal dimension	
		Total fractal dimension	Unitless
		Arteriolar/venular dimension	Unitless
		Bifurcation	
		Arteriolar/venular branching angle	Degrees
		Arteriolar/venular bifurcation index	Unitless
		Arteriolar/venular asymmetry ratio	Unitless
		Arteriolar/venular area ratio	Unitless
		Arteriolar/venular junction exponent	Unitless
Cerebral small-vessel disease	Magnetic resonance imaging	Total WMH volume	mL
		Periventricular WMH volume	mL
		Deep cortical WMH volume	mL
		Lacunar infarcts	No.
		Cerebral microbleeds	No.
Endothelial glycocalyx	Videomicroscopy	Glycocalyx thickness in sublingual microvessels	µm
Plasma and urine biomarkers	Fasting plasma sample	Plasma	
		Von Willebrand factor	%
		Soluble E-selectin	ng/mL
		sICAM1	ng/mL
		sVCAM1	ng/mL
	24-hour urine sample	Urine	
		Albumin excretion	mg/24 hours

Abbreviations: AU, arbitrary units; MU, measurement units; PU, perfusion units; sICAM-1, soluble intercellular adhesion molecule 1; sVCAM-1, soluble vascular cell adhesion molecule 1; WMH, white matter hyperintensity.

[a] Based on the cutpoints of Stefanovska et al. (15).

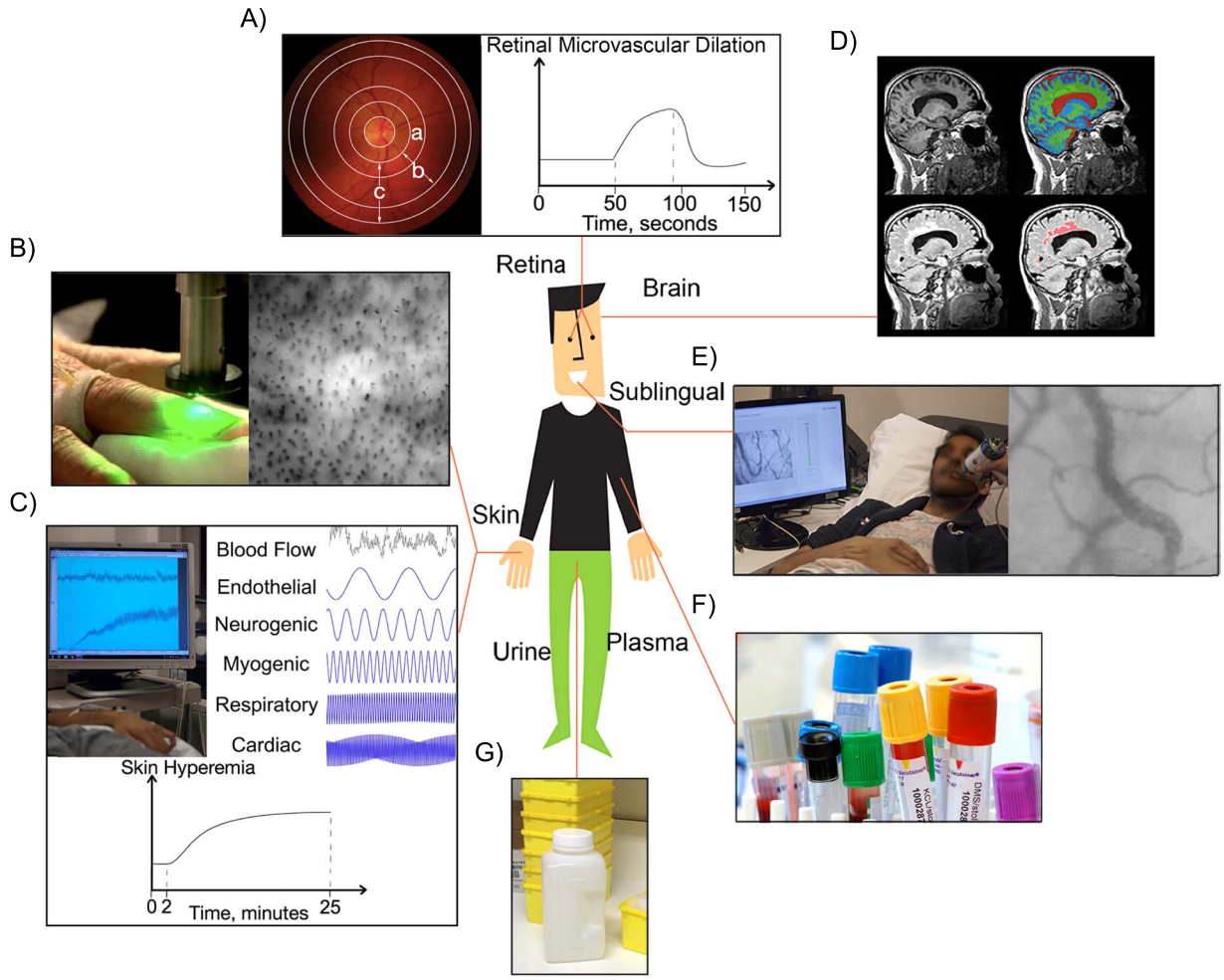

Figure 1. Noninvasive microvascular measurements in the Maastricht Study, Maastricht, the Netherlands, 2010–2018. A) Retinal microvascular diameters and morphology and retinal microvascular reactivity. Left: a typical example of an optic disc-centered image showing the retinal microvasculature. Zones a, b, and c are defined as the regions 1.0–1.5, 1.0–2.5, and 1.0–3.0 disc diameters away from the optic disc center or fovea (macula) center, respectively. Right: schematic registration of a 40-second flicker light-induced retinal arteriolar dilation response using the Dynamic Vessel Analyzer (Imedos Systems GmbH, Jena, Germany). B) Skin capillary density and recruitment. Left: skin capillaries are visualized in the dorsal skin of the distal phalanges of the third and fourth fingers of the right hand by means of a digital video microscope. Right: a typical example of skin capillaries. C) Skin microvascular flowmotion (SMF) and skin heating response. Upper left panel: SMF measurement is performed by use of a laser Doppler system equipped with 2 probes at the dorsal side of both the left wrist and the left ankle. Upper right panel: frequency spectrum of SMF between 0.01 Hz and 1.60 Hz, divided into 5 SMF components based on the cutpoints of Stefanovska et al. (15)): endothelial, 0.01–0.02 Hz; neurogenic, 0.02–0.06 Hz; myogenic, 0.06–0.15 Hz; respiratory, 0.15–0.40 Hz; and cardiac, 0.40–1.60 Hz. Lower panel: schematic registration of a 23-minute heat-induced skin hyperemic response using laser Doppler flowmetry. D) Magnetic resonance imaging markers of cerebral small-vessel disease. Upper left panel: T1-weighted scan. Upper right panel: T1-weighted image with segmented volumes overlaid. Lower left panel: T2-weighted fluid attenuated inversion recovery (FLAIR) scan. Lower right panel: T2-weighted FLAIR image with white matter hyperintensities marked in red. E) Endothelial glycocalyx thickness. Left: sublingual microcirculation is visualized by means of a sidestream dark field camera. Right: a typical example of sublingual microcirculation displayed by videomicroscopy. F) Plasma biomarkers. Venous plasma samples are taken to measure biomarkers of endothelial function. G) Urine biomarkers. Urinary albumin concentration is measured by means of two 24-hour urine collections. Albuminuria is defined as albumin excretion $\geq$30 mg/24 hours.

based features. We measure retinal arteriolar and venular tortuosity using both conventional and exponential methods (30). We calculate fractal dimension on the basis of the box-counting method (31). Calculation of microvascular bifurcation-based features, including branching angles, bifurcation index, asymmetry ratio, area ratio, and junction exponent, has been described elsewhere (32).

Skin capillary density and recruitment

Skin microcirculation is considered a representative vascular bed with which to examine generalized systemic MVD (33). In the Maastricht Study, skin capillaries are visualized in the dorsal skin of the distal phalanges of the third and fourth fingers of the right hand using a digital video

microscope (CapiScope; KK Technology, Honiton, United Kingdom) with a system magnification of ×100 (13). Participants are studied in the supine position with the investigated hand placed at heart level. The finger is fixed on a finger holder, and a miniature cuff (digit cuff; D. E. Hokanson, Inc., Belluvue, Washington) is applied to the base of the investigated finger (Figure 1B, left panel). Capillaries are visualized 4.5 mm proximal to the terminal row of capillaries in the middle of the nailfold, where capillaries run perpendicularly to the skin (Figure 1B, right panel). The investigator selects a region of interest of 1 mm^2 of skin area.

Capillary density (mean of 2 fields) is measured under 3 conditions. First, baseline capillary density, defined as the number of continuously erythrocyte-perfused capillaries per 1 mm^2 of skin, is measured. Capillaries are counted for 15 seconds at baseline. Second, capillary recruitment during postocclusive peak reactive hyperemia is assessed after arterial occlusion. Arterial occlusion is applied using a miniature cuff at the base of the investigated finger inflated to suprasystolic pressure (260 mm Hg) for 4 minutes. Immediately following release of the cuff, all (continuously and intermittently) perfused capillaries are counted for 15 seconds. Third, venous congestion is applied, with the cuff inflated to 60 mm Hg for 2 minutes, and all (continuously and intermittently) perfused capillaries are counted for 15 seconds in the second minute. The number of perfused capillaries is counted in the recorded digital raw data using a custom-built semiautomatic image analysis application (CapiAna) constructed by 2 of the authors (E.H.B.M.G. and A.J.H.M.H.) (13). For analysis, we use absolute numbers of capillaries recorded at baseline, after arterial occlusion, and during venous congestion. In addition, we calculate percentage of capillary recruitment following arterial occlusion ([(capillary density during hyperemia − baseline capillary density)/baseline capillary density] × 100) and percentage of capillary density during venous congestion ([(capillary density during venous congestion − baseline capillary density)/baseline capillary density] × 100).

Skin flowmotion

Flowmotion is the fluctuation of microvascular perfusion as a result of spontaneous oscillations in arteriolar diameter (i.e., vasomotion). Skin microvascular flowmotion (SMF) can be monitored by laser Doppler flowmetry. This technique is based on a fiber-optic probe emitting laser light (wavelength 780 nm) to the target tissue and collecting the back-scattered light, which undergoes a shift in frequency proportional to the velocity of moving erythrocytes. The measuring depth is 0.5–1.0 mm, and the signal is predominantly derived from arterioles and venules (16). We perform SMF measurements using a laser Doppler system (PeriFlux 5000; Perimed AB, Järfälla, Sweden) equipped with 2 probes, one at the dorsal side of the left wrist and the other at the dorsal side of the left ankle (Figure 1C, upper left panel). Since flowmotion has predominantly been observed in participants with a skin temperature above 29.3°C (34), the laser Doppler probes are maintained at 30°C. The laser Doppler flowmetry output is recorded for 25 minutes with a sample rate of 32 Hz, which gives semiquantitative assessment of skin blood flow expressed in arbitrary perfusion units (35).

A fast-Fourier transform algorithm is performed by means of a custom-built automatic software application created in MATLAB (MathWorks, Inc., Natick, Massachusetts) to distinguish the contributions of different frequency domains to the signal. The frequency spectrum between 0.01 Hz and 1.60 Hz is divided into 5 SMF components (using the cutpoints of Stefanovska et al. (15)): endothelial, 0.01–0.02 Hz; neurogenic, 0.02–0.06 Hz; myogenic, 0.06–0.15 Hz; respiratory, 0.15–0.40 Hz; and cardiac, 0.40–1.60 Hz (Figure 1C, upper right panel). The results are presented as power spectrum density, which describes the density of power in a stationary, random process per unit of frequency and can be expressed as (perfusion units)^2 per Hz. Total energy is obtained by the sum of the power density values of the total frequency spectrum. To correct for spatial and temporal variations in the laser Doppler flowmetry signal, the relative contributions of the components are calculated by dividing the power of each component by the power of the total SMF (0.01–1.60 Hz) (36).

Skin heating response

Local heat induces skin hyperemia and increases the skin blood flow. This heat-induced skin response is mainly dependent on nitric oxide and endothelium-derived hyperpolarizing factors (37). To quantify this response, skin blood flow is measured by means of a laser Doppler system (PeriFlux 5000) as described above (Figure 1C, upper left panel). Two thermostatic probes are attached to the wrist and ankle to induce local heating. Skin blood flow is first recorded unheated for 2 minutes to serve as a baseline measure. Next, the temperature of the probe is rapidly and locally increased to 44°C and is then kept constant for the next 23 minutes (Figure 1C, lower panel). The heat-induced skin hyperemic response is expressed as the percentage increase in average perfusion units during the 23-minute heating phase over the average baseline perfusion units.

MRI markers of cerebral small-vessel disease

Brain MVD is reflected by MRI features of cerebral small-vessel disease, including white matter hyperintensities (WMHs), lacunar infarcts, and cerebral microbleeds. In the Maastricht Study, MRI is performed on a 3T MRI scanner (Siemens Magnetom Prisma-Fit Syngo MR D13D; Siemens AG, Erlangen, Germany) using a 64-element head coil for parallel imaging (Figure 1D). The MRI protocol consists of a 3-dimensional T1-weighted sequence (repetition time (TR)/echo time (TE)/inversion time (TI) 2,300 ms/2.98 ms/900 ms, 1.00-mm cubic voxel, 176 continuous slices, matrix size of 240 × 250, and reconstructed matrix size of 512 × 512), a T2-weighted fluid-attenuated inversion recovery (TR/TE/TI 5,000 ms/394 ms/1,800 ms, 0.98 × 0.98 × 1.26-mm acquisition voxel, 0.49 × 0.49 × 1.00-mm reconstructed voxel, 176 continuous slices, acquisition matrix size of 250 × 250, and reconstructed matrix size of 512 × 512), and a gradient

recalled echo pulse sequence with susceptibility-weighted imaging. The protocols for MRI acquisition and analysis are in line with current imaging standards (Standards for Reporting Vascular Changes on Neuroimaging (STRIVE), version 2) (19).

T1-weighted images and T2-weighted fluid-attenuated inversion recovery images are used to identify WMHs by use of an International Organization for Standardization (ISO)-13485 2012-certified automated method (which includes visual inspection) (38). Numbers of all WMHs identified are summed for assessment of total WMH burden in milliliters. Periventricular WMHs are automatically defined as WMHs less than 3 mm from the cerebrospinal fluid and deep cortical WMHs as WMHs 3 or more mm from the cerebrospinal fluid (39). This method has a small chance of misclassifying juxtacortical WMHs, which are relatively uncommon (40), as periventricular WMHs. The location and number of lacunar infarcts are manually rated on T2 and fluid-attenuated inversion recovery images and defined as focal lesions of $\geq$3 mm and $<$15 mm in size with a similar signal intensity as cerebrospinal fluid on all sequences and a hyperintense rim (19). The location and number of cerebral microbleeds are manually rated on 3-dimensional T2$*$ gradient recalled echo-weighted imaging with susceptibility-weighted imaging by means of the Microbleed Anatomical Rating Scale (41) and defined as focal lesions of $\geq$2 mm and $\leq$10 mm in size with a hypointense signal on T2$*$ gradient recalled echo- and susceptibility-weighted images (19). Three neuroradiologists perform the rating of lacunar infarcts and cerebral microbleeds.

Endothelial glycocalyx thickness

The glycocalyx is a gel layer on the luminal side of endothelial cells which prevents blood cells from penetrating or adhering to the vessel wall. Impaired glycocalyx function would allow more red blood cells (RBCs) to penetrate deeper towards the endothelial surface, which may influence endothelial function (42). We use the Glycocheck system (Microvascular Health Solutions, Inc., Salt Lake City, Utah) to measure glycocalyx thickness in the sublingual microcirculation (Figure 1E). After calibration, the lens is placed against the lingual frenum near the tongue base with limited pressure. The sidestream dark field camera uses green light-emitting diodes (540 nm) to detect the hemoglobin of passing RBCs. All measurable vessels are identified, recorded, and analyzed automatically. Vessels with RBC columns larger than 30 μm in diameter or high tortuosity are excluded.

The results of analyses are presented as the perfused boundary region (μm), which is calculated as the distance between the outer boundaries of the erythrocytes and the center lumen of the vessel ((perfused diameter − median RBC column width)/2) (20). It reflects the dynamic lateral position of RBCs. Then the calculated perfused boundary region values, classified according to their corresponding RBC column widths between 5 μm and 25 μm, are averaged to provide a single perfused boundary region value for each participant.

Plasma and urine biomarkers

Since microvascular endothelium covers approximately 98% of the total vascular surface area and synthetic capacity (21), plasma or serum biomarkers of endothelial function, such as soluble vascular cell adhesion molecule 1, soluble intercellular adhesion molecule 1, soluble E-selectin, and von Willebrand factor, can be regarded as reflecting mainly microvascular endothelial function. Among these, soluble vascular cell adhesion molecule 1, soluble intercellular adhesion molecule 1, and soluble E-selectin are measured in ethylenediaminetetraacetic acid plasma samples with commercially available 4-plex sandwich immunoassay kits (Meso Scale Discovery, Rockville, Maryland) as described previously (43). Von Willebrand factor is quantified in citrate plasma using an enzyme-linked immunosorbent assay (Dako Denmark A/S, Glostrup, Denmark). Concentrations of von Willebrand factor are expressed as a percentage of von Willebrand factor detected in pooled citrated plasma of healthy volunteers (Figure 1F).

Albuminuria can be regarded as a marker of generalized endothelial dysfunction (3). To assess urinary albumin excretion, participants are requested to collect two 24-hour urine samples (Figure 1G). Urinary albumin concentration is measured with a standard immunoturbidimetric assay by means of an automatic analyzer (Beckman Synchron LX20; Beckman Coulter, Inc., Brea, California) and multiplied by collection volume to obtain 24-hour urinary albumin excretion. A urinary albumin concentration below the detection limit of the assay (2 mg/L) is set at 1.5 mg/L before multiplying by collection volume. Only urine collections with a collection time between 20 hours and 28 hours are considered valid. If needed, urinary albumin excretion is extrapolated to a 24-hour excretion. Microalbuminuria is defined as a 24-hour albumin excretion of 30–300 mg/24 hours, and macroalbuminuria is defined as a 24-hour albumin excretion greater than 300 mg/24 hours. These definitions are preferably based on the average of two 24-hour urine collections (available for approximately 90% of the participants).

Validation of measurements

Validation of measurements is described in the Web Appendix.

RESULTS

Currently, we have carried out a number of cross-sectional investigations involving microvascular measurements within the framework of the Maastricht Study and have found that multiple cardiovascular risk factors (age, sex, blood pressure, waist circumference, etc.) and diseases (e.g., (pre)diabetes and depression) are associated with microvascular (dys)function. The findings are summarized in Tables 2 and 3.

Cardiovascular risk factors and microvascular function

MVD may be a common pathological phenomenon in cardiovascular diseases that is induced by multiple risk

Table 2. Associations of Cardiovascular Risk Factors with Microvascular Function in the Maastricht Study, Maastricht, the Netherlands, 2010–2018

Risk Factor (Reference No.)	Associated Microvascular Marker			
	Skin Flowmotion	Heat-Induced Skin Hyperemia	Flicker Light-Induced Retinal Microvascular Reactivity	Cerebral Small-Vessel Disease
Older age (44, 45)	Higher total power density Higher respiratory power density Higher cardiac power density	Lower hyperemic response	Lower retinal arteriolar dilation	NA
Male sex (44, 45)	No significant association	Lower hyperemic response	No significant association	NA
Greater waist circumference and body mass index[a] (44, 45)	Lower total power density	No significant association	No significant association	NA
Current smoking (44, 45)	No significant association	Lower hyperemic response	No significant association	NA
Higher blood pressure (44, 45)	Higher total power density	Lower hyperemic response	Higher retinal arteriolar dilation	NA
Higher plasma glucose concentration (44–47)	No significant association	Lower hyperemic response	Lower retinal arteriolar dilation	Larger total WMH volume Larger periventricular WMH volume Larger deep cortical WMH volume Presence of lacunar infarcts

Abbreviations: NA, not (yet) assessed in the Maastricht Study; WMH, white matter hyperintensity.
[a] Weight (kg)/height $(m)^2$.

factors. In a preliminary study with a limited number of participants, we used skin flowmotion measurement and found that older age and higher 24-hour systolic blood pressure were associated with a higher total SMF energy, while greater waist circumference and body mass index (weight (kg)/height $(m)^2$) were associated with a lower total SMF energy (44). Further analysis of the 5 frequency components revealed associations of older age with higher energy contributions of the respiratory and cardiac components and of higher 24-hour systolic blood pressure with higher energy contributions of all 5 frequency components, as well as associations of greater waist circumference with lower energy contributions of all of the frequency components (44).

Evaluating microvascular responses in skin and retina, we observed that older age and higher plasma glucose level were associated with both lower heat-induced skin hyperemia and lower flicker light-induced retinal arteriolar dilation (45, 46). In addition, lower heat-induced skin hyperemia was found in men and in current smokers (45). Interestingly, we did not find any association of 24-hour systolic blood pressure with microvascular responses in skin or retina. Instead, higher 24-hour pulse pressure was associated with lower heat-induced skin hyperemia, and higher 24-hour diastolic blood pressure was associated with increased flicker light-induced retinal arteriolar dilation (45). Higher plasma glucose level was associated with the presence of brain lacunar infarcts and larger volumes of WMHs, including deep cortical and periventricular WMHs, but not with the presence of cerebral microbleeds (47).

In addition, arterial stiffening as determined by carotid-femoral pulse wave velocity was not associated with skin capillary density or recruitment, skin flowmotion, or heat-induced skin hyperemia, as demonstrated in analyses carried out in both the Maastricht Study and Supplementation en Vitamines et Mineraux Antioxydants 2 (SU.VI.MAX2) Study cohorts (48).

Chronic diseases and microvascular function

The "ticking clock" hypothesis postulates that the clock for coronary heart disease development starts ticking before the onset of clinical diabetes (49). Similarly, T2DM-associated MVD may occur long before T2DM is diagnosed. In view of this, we studied the association between glucose metabolism status and MVD. We found that both impaired flicker light-induced retinal arteriolar

Table 3. Associations of Chronic Diseases with Microvascular Function in the Maastricht Study, Maastricht, the Netherlands, 2010–2018

Condition or Organ and Outcome (Reference No.)	Associated Microvascular Marker				
	Skin Capillary Density and Recruitment	Heat-Induced Skin Hyperemia	Flicker Light-Induced Retinal Microvascular Reactivity	Plasma and Urine Biomarkers	Cerebral Small-Vessel Disease
Diabetic conditions					
Prediabetes (46, 47)	NA	Lower hyperemic response	Lower retinal arteriolar dilation	NA	Larger total WMH volume Larger periventricular WMH volume Larger deep cortical WMH volume Presence of lacunar infarcts
Type 2 diabetes mellitus (46, 47)	NA	Lower hyperemic response	Lower retinal arteriolar dilation	NA	Larger total WMH volume Larger periventricular WMH volume Larger deep cortical WMH volume Larger lacunar infarcts
Brain					
Depressive disorder/ symptoms (43)	NA	NA	NA	Higher endothelial dysfunction summary score (consisting of sVCAM-1, sICAM-1, soluble E-selectin, and von Willebrand factor)	NA
Cognitive performance (52)	NA	NA	NA	Albuminuria[a]	NA
Kidney					
Albuminuria[a] (55, 56)	Lower recruitment following arterial occlusion Lower recruitment during venous congestion	Lower hyperemic response	Lower retinal arteriolar dilation	NA	NA

Abbreviations: NA, not (yet) assessed in the Maastricht Study; sICAM-1, soluble intercellular adhesion molecule 1; sVCAM-1, soluble vascular cell adhesion molecule 1; WMH, white matter hyperintensity.

[a] Note that albuminuria can be a marker of both microvascular dysfunction and outcome and is defined as urinary albumin excretion ≥30 mg/24 hours.

dilation and heat-induced skin hyperemia have already occurred in prediabetes (defined as impaired fasting glucose concentration and/or impaired glucose tolerance), and both impairments were more severe in established T2DM (46). Prediabetes and T2DM were also associated with markers of cerebral small-vessel disease, including the presence of lacunar infarcts, and larger volumes of WMHs, as compared with normal glucose metabolism (47). In contrast, there were no significant associations of prediabetes and T2DM with the presence of cerebral microbleeds (47). To explore the underlying mechanism of (pre)diabetes-associated MVD, we further performed mediation analysis and found that,

among hyperglycemia, insulin resistance, blood pressure, lipid profile, and low-grade inflammation, hyperglycemia was the main mediator of both the prediabetes-associated and T2DM-associated skin and retinal MVD, with a mediation effect of approximately 50%–75% (50).

Depression and cognitive decline are thought to be partly related to MVD (51). In a recent meta-analysis, we provided evidence that not only cerebral forms of MVD but also peripheral MVD, as measured by plasma biomarkers, is associated with incident depression (6). In the Maastricht Study, we also found higher levels of plasma markers of endothelial dysfunction to be associated with the presence of depressive disorder and a higher depressive symptom score (43). With regard to cognitive function, albuminuria, defined as urinary albumin excretion ≥30 mg/24 hours, was associated with lower information processing speed, independent of educational level, cardiovascular risk factors, and lifestyle factors (52). This association tended to be stronger in older individuals (52).

Albuminuria, normally considered a measure of kidney dysfunction, is also thought to reflect generalized endothelial dysfunction. However, this hypothesis has been tested only with indirect measurements, such as plasma biomarkers of endothelial function (53, 54). Therefore, we examined the association of direct measurements of MVD in skin and retina with albuminuria. We found that lower skin capillary recruitment following arterial and venous occlusion was associated with the presence of albuminuria (55). Lower flicker light-induced retinal arteriolar dilation was also associated with albuminuria, and this association was stronger in persons with T2DM. In addition, the association of lower heat-induced skin hyperemic response with albuminuria was present in persons with T2DM only (56). These findings suggested an interaction effect of T2DM on the association between direct measurements of MVD and albuminuria.

DISCUSSION

For the development of both prevention and treatment strategies in the general population, we need solid epidemiologic data. To our knowledge, no population-based study has applied a wide scope of microvascular morphological and functional phenotyping. Most studies have applied, at most, a few of the microvascular measurements discussed here, including plasma biomarkers, retinal microvascular diameters, and cerebral small-vessel disease (2, 6). In the Maastricht Study (22), we combine an array of microvascular measurements in different vascular beds (e.g., low and high flow impedance) with extensive phenotyping of biometric factors, lifestyle and cardiovascular risk factors, and diseases. This approach allows us to study not only the role of generalized MVD in the development and progression of various diseases with a systems physiology approach but also MVD, which is specific for certain organs/tissues (Figure 2).

In the Maastricht Study, we have observed associations of MVD with cardiovascular risk factors, (pre)diabetes, depression, cognitive function, and albuminuria. These results suggest that 1) microvascular function is determined by multiple cardiovascular risk factors (44–47), 2) MVD occurs prior to the diagnosis of T2DM (46, 47), 3) MVD is a systemic pathophysiological phenomenon in T2DM, and 4) MVD is associated with (end)organ dysfunction (e.g., depression, cognitive decline, albuminuria) (43, 52, 55, 56).

Strengths of the Maastricht Study

The combination of an array of microvascular measurements and the extensive phenotyping in the Maastricht Study has several strengths. First, the size of the study population in conjunction with the extensive phenotyping enables detection of independent associations after extensive adjustment for potential confounders. Second, the standard operating procedures and the quality control over time enhance the consistency of the microvascular measurements and increase their usability in other studies. Third, the use of multiple microvascular measurements enables comparison of changes in the microvasculature across arterioles, capillaries, and venules, as well as across territories, in order to disentangle the influence of risk factors/diseases on the microvasculature as well as the heterogeneity of the microvasculature responding to different (patho)physiological situations (57).

Longitudinal studies

Currently, annual follow-up on disease incidence and mortality is being performed in the Maastricht Study, which will enable longitudinal analyses. Through the cross-sectional studies, we have already found that MVD in multiple territories is present before the diagnosis of T2DM (prediabetes), which implies that MVD is not only a consequence of T2DM but also an essential factor that can precede T2DM and increase the risk of its complications and comorbidities, which are partly of microvascular origin. To confirm this, longitudinal studies are planned to investigate the association of MVD with the incidence of various diseases, such as T2DM, cardiovascular diseases, and cerebral diseases. In addition, microvascular measurements will be included in the follow-up procedure to investigate the microvascular changes with development and progression of diseases.

Fully automated analysis of microvascular imaging

Several microvascular measurements are based on imaging, of which the analyses are often performed manually. To apply such measurements efficiently in a population-based setting requires fully automated analysis software. Recent technical advances have enabled a transition from manual/semiautomated image analysis to fully automated image analysis and have made this approach more precise and time-saving (e.g., the software for detecting brain WMHs in the Maastricht Study) (38). In addition, this approach allows identification, extraction, and investigation of novel microvascular features, such as retinal microvascular tortuosity, fractal dimension, and bifurcation features. These

developments provide for a more comprehensive observation of microvascular changes as well as better availability and implementation of the microvascular measurements in a large population, for either research or clinical use. Further, the protocols involving image acquisition, processing, and analysis should be standardized across studies, and reproducibility and validity should be carefully documented, for use by other researchers and further applications.

The first wave of data collection in the Maastricht Study (including more than 9,000 participants) continued through 2019. Next, we plan to start follow-up surveys in the same cohort. In the coming years, we will develop, validate, and implement fully automated image analysis applications. In that way, a wealth of different microvascular morphological and functional markers of different territories will become available. It is important to assess the associations and role of MVD in relation to disease development in order to assess whether interventions against MVD should be developed for prevention purposes.

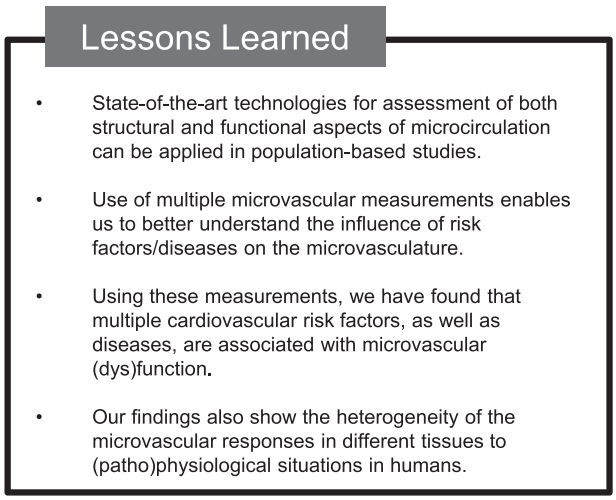

Figure 2. Lessons learned from microvascular phenotyping in the Maastricht Study, Maastricht, the Netherlands, 2010–2018.

ACKNOWLEDGMENTS

Author affiliations: Department of Internal Medicine, School for Cardiovascular Diseases, Maastricht University Medical Center+, Maastricht, the Netherlands (Wenjie Li, Miranda T. Schram, Ben M. Sörensen, Marnix J. M. van Agtmaal, Casper G. Schalkwijk, Coen D. A. Stehouwer, Alfons J. H. M. Houben); University Eye Clinic Maastricht, Maastricht University Medical Center+, Maastricht, the Netherlands (Tos T. J. M. Berendschot, Carroll A. B. Webers); Department of Radiology and Nuclear Medicine, Maastricht University Medical Center+, Maastricht, the Netherlands (Jacobus F. A. Jansen, Walter H. Backes); and Department of Psychiatry and Neuropsychology, School for Mental Health and Neuroscience, Maastricht University Medical Center+, Maastricht, the Netherlands (Walter H. Backes, Ed H. B. M. Gronenschild).

This study was supported by the European Regional Development Fund via Operationele Programma Zuid, the Province of Limburg, the Dutch Ministry of Economic Affairs (grant 310.041), the De Weijerhorst Foundation (Maastricht, the Netherlands), the Pearl String Initiative Diabetes (Amsterdam, the Netherlands), the School for Cardiovascular Diseases at Maastricht University Medical Center+ (Maastricht, the Netherlands), the Care and Public Health Research Institute of Maastricht University Medical Center+ (Maastricht, the Netherlands), the School of Nutrition and Translational Research in Metabolism of Maastricht University Medical Center+ (Maastricht, the Netherlands), the Annadal Foundation (Maastricht, the Netherlands), Health Foundation Limburg (Maastricht, the Netherlands), and Perimed AB (Järfalla, Sweden), as well as by unrestricted grants from Janssen-Cilag BV (Tilburg, the Netherlands), Novo Nordisk Farma BV (Alphen aan den Rijn, the Netherlands) and Sanofi-Aventis Netherlands BV (Gouda, the Netherlands). W.L. was supported by the Chinese Scholarship Council (grant 201606260039).

The Regional Association of General Practitioners (Zorg in Ontwikkeling) is gratefully acknowledged for their contribution to the Maastricht Study, enabling the invitation of persons with type 2 diabetes through the use of information from their Web-based electronic health records.

Conflict of interest: none declared.

REFERENCES

1. Houben A, Martens RJH, Stehouwer CDA. Assessing microvascular function in humans from a chronic disease perspective. *J Am Soc Nephrol*. 2017;28(12):3461–3472.
2. Muris DM, Houben AJ, Schram MT, et al. Microvascular dysfunction is associated with a higher incidence of type 2 diabetes mellitus: a systematic review and meta-analysis. *Arterioscler Thromb Vasc Biol*. 2012;32(12): 3082–3094.
3. Stehouwer CD. Microvascular dysfunction and hyperglycemia: a vicious cycle with widespread consequences. *Diabetes*. 2018;67(9):1729–1741.
4. Lee JF, Barrett-O'Keefe Z, Garten RS, et al. Evidence of microvascular dysfunction in heart failure with preserved ejection fraction. *Heart*. 2016;102(4):278–284.
5. Stehouwer CD, Smulders YM. Microalbuminuria and risk for cardiovascular disease: analysis of potential mechanisms. *J Am Soc Nephrol*. 2006;17(8):2106–2111.
6. van Agtmaal MJM, Houben A, Pouwer F, et al. Association of microvascular dysfunction with late-life depression: a systematic review and meta-analysis. *JAMA Psychiatry*. 2017;74(7):729–739.
7. Danese S, Dejana E, Fiocchi C. Immune regulation by microvascular endothelial cells: directing innate and adaptive immunity, coagulation, and inflammation. *J Immunol*. 2007; 178(10):6017–6022.
8. Drachman DA, Smith TW, Alkamachi B, et al. Microvascular changes in Down syndrome with Alzheimer's-type pathology: insights into a potential vascular mechanism for Down syndrome and Alzheimer's disease. *Alzheimers Dement*. 2017;13(12):1389–1396.

9. De Boer MP, Meijer RI, Wijnstok NJ, et al. Microvascular dysfunction: a potential mechanism in the pathogenesis of obesity-associated insulin resistance and hypertension. *Microcirculation*. 2012;19(1):5–18.
10. Houben AJ, Eringa EC, Jonk AM, et al. Perivascular fat and the microcirculation: relevance to insulin resistance, diabetes, and cardiovascular disease. *Curr Cardiovasc Risk Rep*. 2012; 6(1):80–90.
11. Levy BI, Ambrosio G, Pries AR, et al. Microcirculation in hypertension: a new target for treatment? *Circulation*. 2001; 104(6):735–740.
12. Aird WC. Phenotypic heterogeneity of the endothelium: I. structure, function, and mechanisms. *Circ Res*. 2007;100(2): 158–173.
13. Gronenschild EH, Muris DM, Schram MT, et al. Semi-automatic assessment of skin capillary density: proof of principle and validation. *Microvasc Res*. 2013;90:192–198.
14. Kvandal P, Landsverk SA, Bernjak A, et al. Low-frequency oscillations of the laser Doppler perfusion signal in human skin. *Microvasc Res*. 2006;72(3):120–127.
15. Stefanovska A, Bracic M, Kvernmo HD. Wavelet analysis of oscillations in the peripheral blood circulation measured by laser Doppler technique. *IEEE Trans Biomed Eng*. 1999; 46(10):1230–1239.
16. Nagel E, Vilser W. Flicker observation light induces diameter response in retinal arterioles: a clinical methodological study. *Br J Ophthalmol*. 2004;88(1):54–56.
17. Romeny BMT, Bekkers EJ, Zhang J, et al. Brain-inspired algorithms for retinal image analysis. *Mach Vis Appl*. 2016; 27(8):1117–1135.
18. Bekkers E, Duits R, Berendschot T, et al. A multi-orientation analysis approach to retinal vessel tracking. *J Math Imaging Vis*. 2014;49(3):583–610.
19. Wardlaw JM, Smith EE, Biessels GJ, et al. Neuroimaging standards for research into small vessel disease and its contribution to ageing and neurodegeneration. *Lancet Neurol*. 2013;12(8):822–838.
20. Nieuwdorp M, Meuwese MC, Mooij HL, et al. Measuring endothelial glycocalyx dimensions in humans: a potential novel tool to monitor vascular vulnerability. *J Appl Physiol (1985)*. 2008;104(3):845–852.
21. Schram MT, Stehouwer CD. Endothelial dysfunction, cellular adhesion molecules and the metabolic syndrome. *Horm Metab Res*. 2005;37(suppl 1):49–55.
22. Schram MT, Sep SJ, van der Kallen CJ, et al. The Maastricht Study: an extensive phenotyping study on determinants of type 2 diabetes, its complications and its comorbidities. *Eur J Epidemiol*. 2014;29(6):439–451.
23. Dorner GT, Garhofer G, Kiss B, et al. Nitric oxide regulates retinal vascular tone in humans. *Am J Physiol Heart Circ Physiol*. 2003;285(2):H631–H636.
24. Garhofer G, Bek T, Boehm AG, et al. Use of the retinal vessel analyzer in ocular blood flow research. *Acta Ophthalmol*. 2010;88(7):717–722.
25. Nagel E, Vilser W, Lanzl I. Age, blood pressure, and vessel diameter as factors influencing the arterial retinal flicker response. *Invest Ophthalmol Vis Sci*. 2004;45(5):1486–1492.
26. Kotliar KE, Lanzl IM, Schmidt-Trucksäss A, et al. Dynamic retinal vessel response to flicker in obesity: a methodological approach. *Microvasc Res*. 2011;81(1):123–128.
27. Nagel E, Vilser W, Fink A, et al. Varianz der Netzhautgefäßreaktion auf Flickerlicht. Eine klinisch-methodische Studie. [Variance of retinal vessel diameter response to flicker light. A methodical clinical study]. *Ophthalmologe*. 2006;103(2): 114–119.
28. Williams TD, Wilkinson JM. Position of the fovea centralis with respect to the optic nerve head. *Optom Vis Sci*. 1992; 69(5):369–377.
29. Knudtson MD, Lee KE, Hubbard LD, et al. Revised formulas for summarizing retinal vessel diameters. *Curr Eye Res*. 2003;27(3):143–149.
30. Bekkers EJ, Zhang J, Duits R, et al. Curvature based biomarkers for diabetic retinopathy via exponential curve fits in SE (2). In: Chen X, Garvin MK, Liu JJ, et al., eds. *Proceedings of the Ophthalmic Medical Image Analysis Second International Workshop, OMIA 2015, Held in Conjunction with MICCAI 2015, Munich, Germany, October 9, 2015*. Iowa City, IA: University of Iowa; 2016:113–120.
31. Masters BR. Fractal analysis of the vascular tree in the human retina. *Annu Rev Biomed Eng*. 2004;6:427–452.
32. Al-Diri B, Hunter A, Steel D, et al. Manual measurement of retinal bifurcation features. *Conf Proc IEEE Eng Med Biol Soc*. 2010;2010:4760–4764.
33. Hellmann M, Roustit M, Cracowski JL. Skin microvascular endothelial function as a biomarker in cardiovascular diseases? *Pharmacol Rep*. 2015;67(4):803–810.
34. Thorn CE, Kyte H, Slaff DW, et al. An association between vasomotion and oxygen extraction. *Am J Physiol Heart C*. 2011;301(2):H442–H449.
35. Braverman IM, Schechner JS, Silverman DG, et al. Topographic mapping of the cutaneous microcirculation using two outputs of laser-Doppler flowmetry: flux and the concentration of moving blood cells. *Microvasc Res*. 1992; 44(1):33–48.
36. Graaff R, Morales F, Smit AJ, et al. Normalization of vasomotion in laser Doppler perfusion monitoring. *Conf Proc IEEE Eng Med Biol Soc*. 2007;2007:4076–4079.
37. Choi PJ, Brunt VE, Fujii N, et al. New approach to measure cutaneous microvascular function: an improved test of NO-mediated vasodilation by thermal hyperemia. *J Appl Physiol (1985)*. 2014;117(3):277–283.
38. de Boer R, Vrooman HA, van der Lijn F, et al. White matter lesion extension to automatic brain tissue segmentation on MRI. *Neuroimage*. 2009;45(4):1151–1161.
39. Kim KW, MacFall JR, Payne ME. Classification of white matter lesions on magnetic resonance imaging in elderly persons. *Biol Psychiatry*. 2008;64(4):273–280.
40. Decarli C, Fletcher E, Ramey V, et al. Anatomical mapping of white matter hyperintensities (WMH) exploring the relationships between periventricular WMH, deep WMH, and total WMH burden. *Stroke*. 2005;36(1):50–55.
41. Gregoire SM, Chaudhary UJ, Brown MM, et al. The Microbleed Anatomical Rating Scale (MARS): reliability of a tool to map brain microbleeds. *Neurology*. 2009;73(21): 1759–1766.
42. Lee DH, Dane MJC, van den Berg BM, et al. Deeper penetration of erythrocytes into the endothelial glycocalyx is associated with impaired microvascular perfusion. *PLoS One*. 2014;9(5):e96477.
43. van Dooren FEP, Schram MT, Schalkwijk CG, et al. Associations of low grade inflammation and endothelial dysfunction with depression—the Maastricht Study. *Brain Behav Immun*. 2016;56:390–396.
44. Muris DM, Houben AJ, Kroon AA, et al. Age, waist circumference, and blood pressure are associated with skin microvascular flow motion: the Maastricht Study. *J Hypertens*. 2014;32(12):2439–2449.
45. Sörensen BM, Houben AJHM, Berendschot TTJM, et al. Cardiovascular risk factors as determinants of retinal and skin microvascular function: the Maastricht Study. *PLoS One*. 2017;12(10):e0187324.

46. Sörensen BM, Houben AJHM, Berendschot TTJM, et al. Prediabetes and type 2 diabetes are associated with generalized microvascular dysfunction: the Maastricht Study. *Circulation*. 2016;134(18):1339–1352.
47. van Agtmaal MJ, Houben AJHM, de Wit V, et al. Prediabetes is associated with structural brain abnormalities: the Maastricht Study. *Diabetes Care*. 2018;41(12):2535–2543.
48. van Sloten TT, Czernichow S, Houben AJ, et al. Association between arterial stiffness and skin microvascular function: the SUVIMAX2 Study and the Maastricht Study. *Am J Hypertens*. 2015;28(7):868–876.
49. Wong MS, Gu K, Heng D, et al. The Singapore Impaired Glucose Tolerance Follow-up Study: does the ticking clock go backward as well as forward? *Diabetes Care*. 2003; 26(11):3024–3030.
50. Sörensen BM, Houben AJHM, Berendschot TTJM, et al. Hyperglycemia is the main mediator of prediabetes- and type 2 diabetes-associated impairment of microvascular function: the Maastricht Study. *Diabetes Care*. 2017;40(8):e103–e105.
51. Taylor WD, Aizenstein HJ, Alexopoulos GS. The vascular depression hypothesis: mechanisms linking vascular disease with depression. *Mol Psychiatry*. 2013;18(9):963–974.
52. Martens RJ, Kooman JP, Stehouwer CD, et al. Estimated GFR, albuminuria, and cognitive performance: the Maastricht Study. *Am J Kidney Dis*. 2017;69(2):179–191.
53. Persson F, Rossing P, Hovind P, et al. Endothelial dysfunction and inflammation predict development of diabetic nephropathy in the Irbesartan in Patients with Type 2 Diabetes and Microalbuminuria (IRMA 2) Study. *Scand J Clin Lab Invest*. 2008;68(8):731–738.
54. Stehouwer CDA, Gall MA, Twisk JW, et al. Increased urinary albumin excretion, endothelial dysfunction, and chronic low-grade inflammation in type 2 diabetes: progressive, interrelated, and independently associated with risk of death. *Diabetes*. 2002;51(4):1157–1165.
55. Martens RJ, Henry RM, Houben AJ, et al. Capillary rarefaction associates with albuminuria: the Maastricht Study. *J Am Soc Nephrol*. 2016;27(12):3748–3757.
56. Martens RJH, Houben AJHM, Kooman JP, et al. Microvascular endothelial dysfunction is associated with albuminuria: the Maastricht Study. *J Hypertens*. 2018;36(5): 1178–1187.
57. Aird WC. Phenotypic heterogeneity of the endothelium: II. Representative vascular beds. *Circ Res*. 2007;100(2):174–190.